Supplementary Data
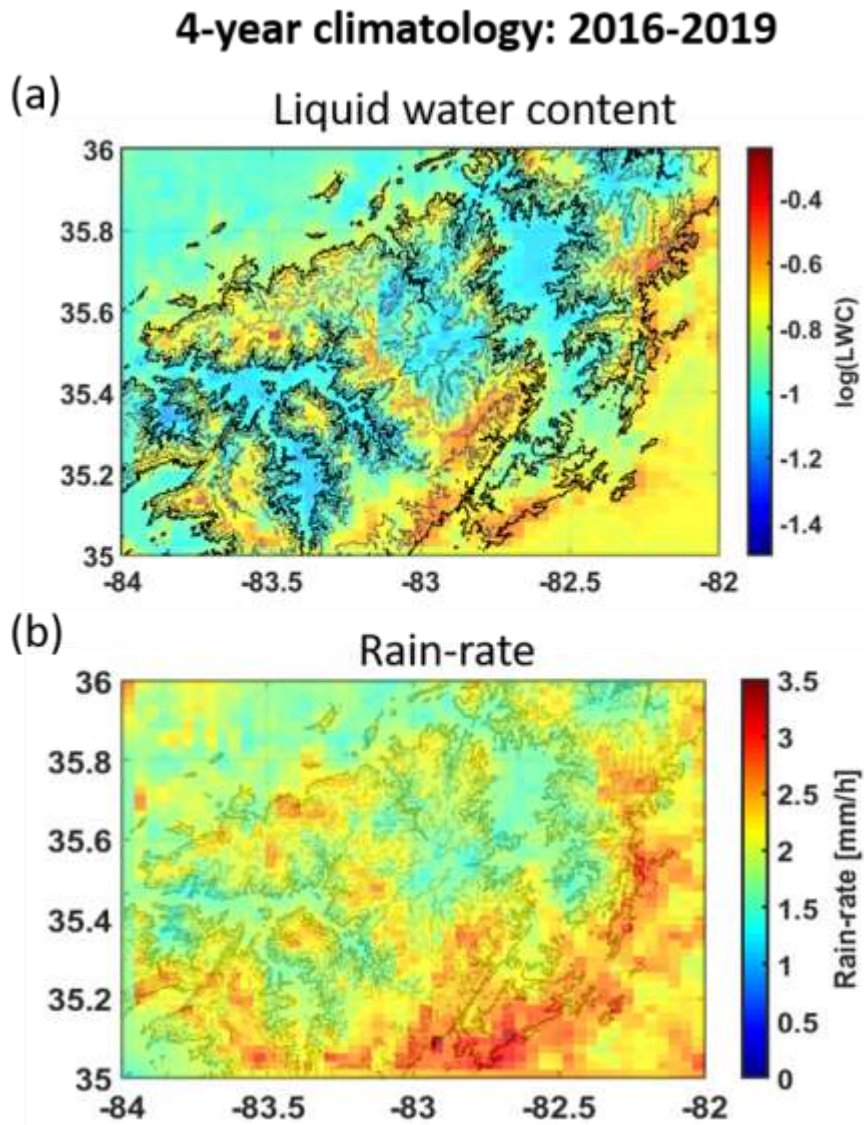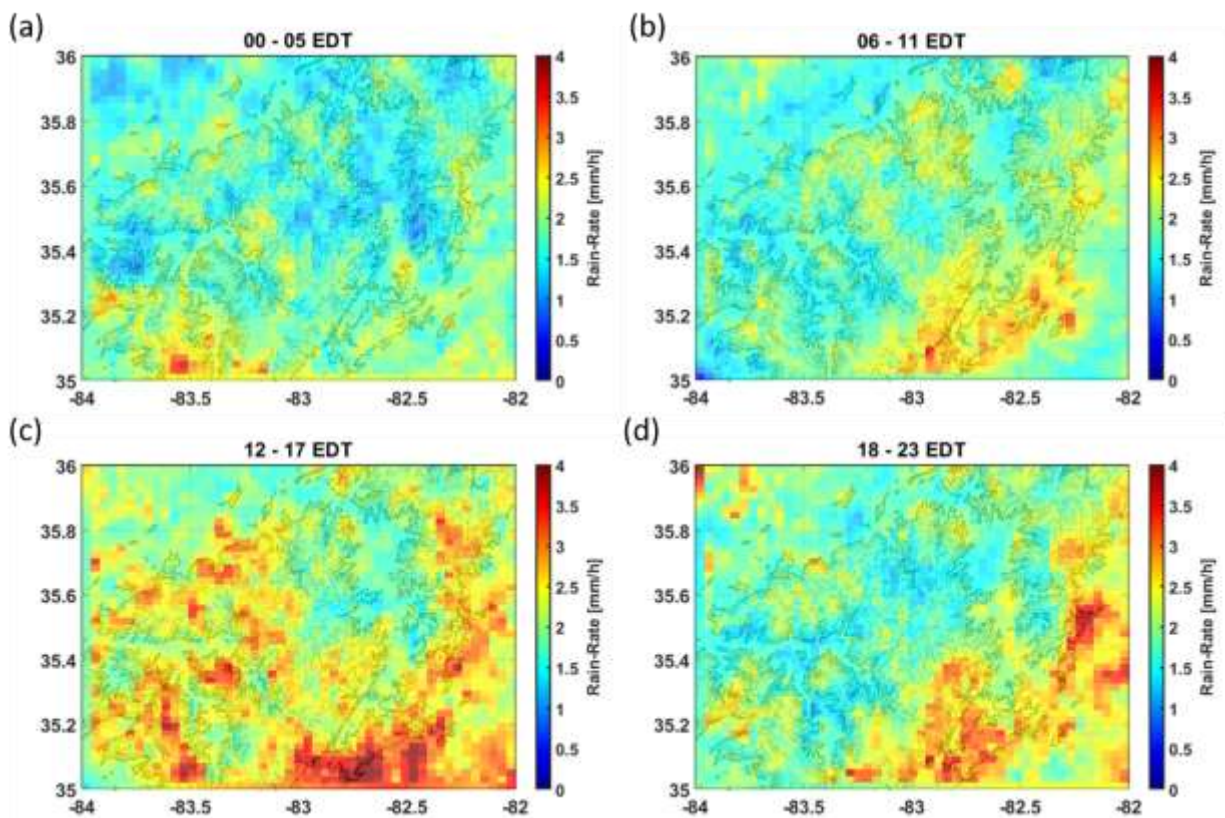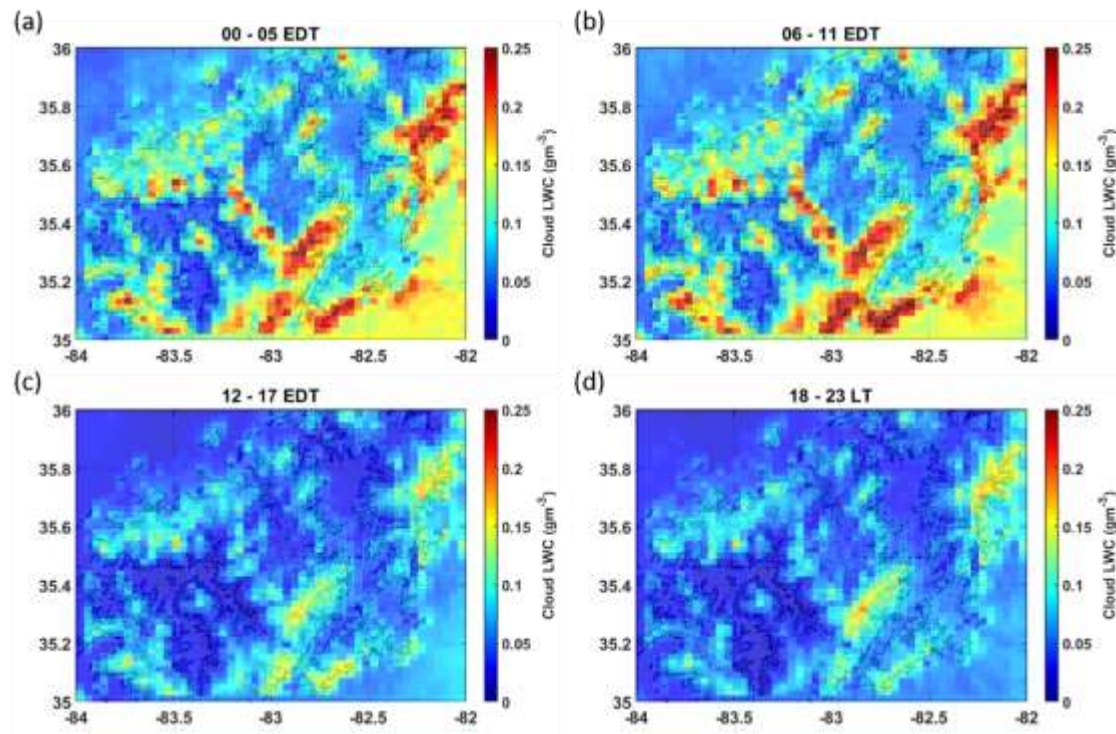

Figure S1. Four-year climatology of (a) Liquid water content and (b) Rain-rate at 500 m AGL estimated by HRRR in the summer (May-October).
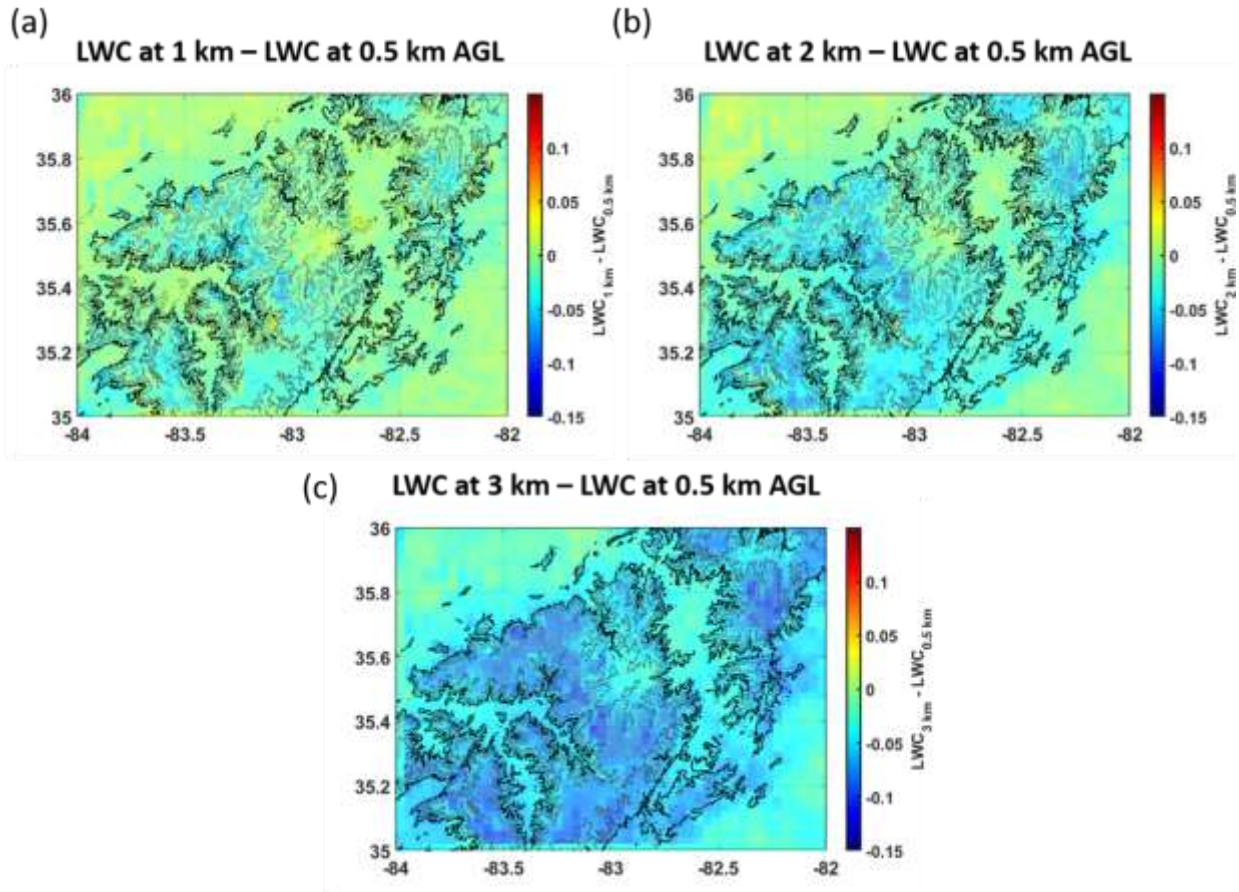
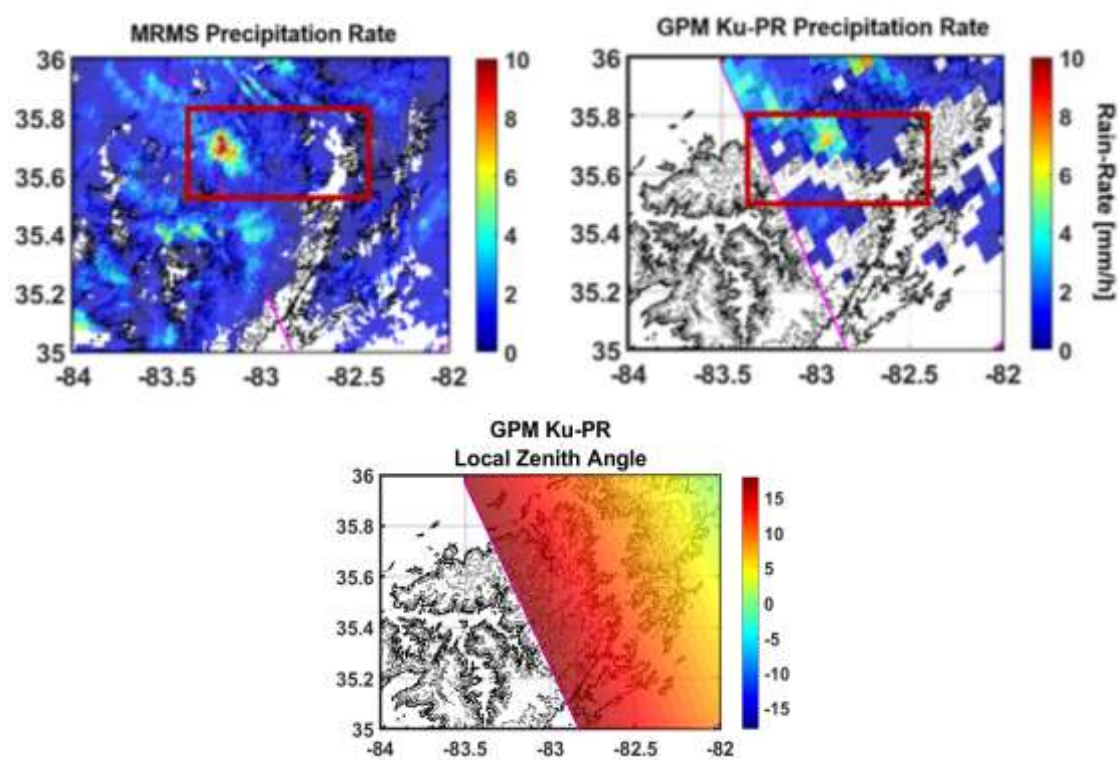**Figure S2.** Diurnal cycle of the HRRR rain-rate climatology at 500 AGL in summer (May-October).

Figure S3. Diurnal cycle 4-year climatology of HRRR estimated cloud-water mixing ratio at 500 m AGL in summer months (May-October).
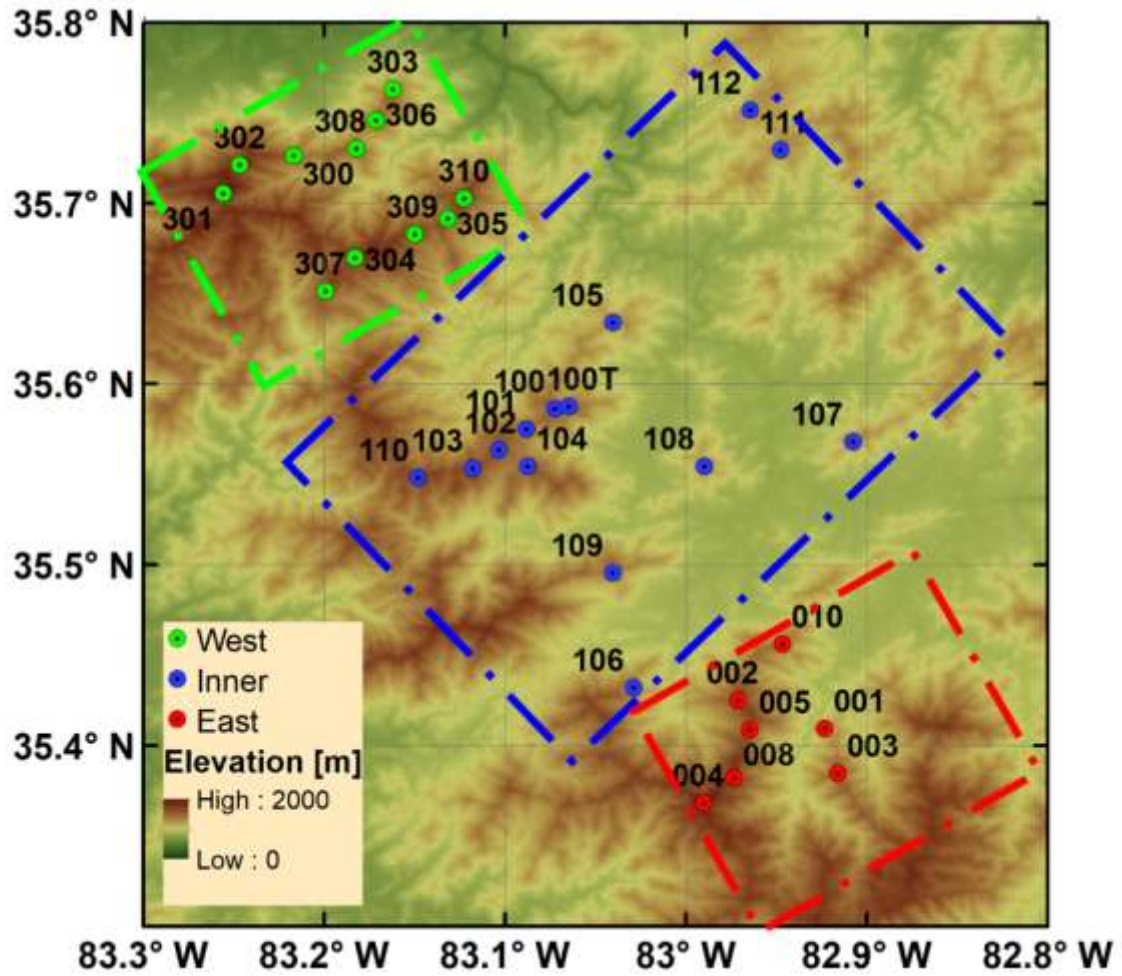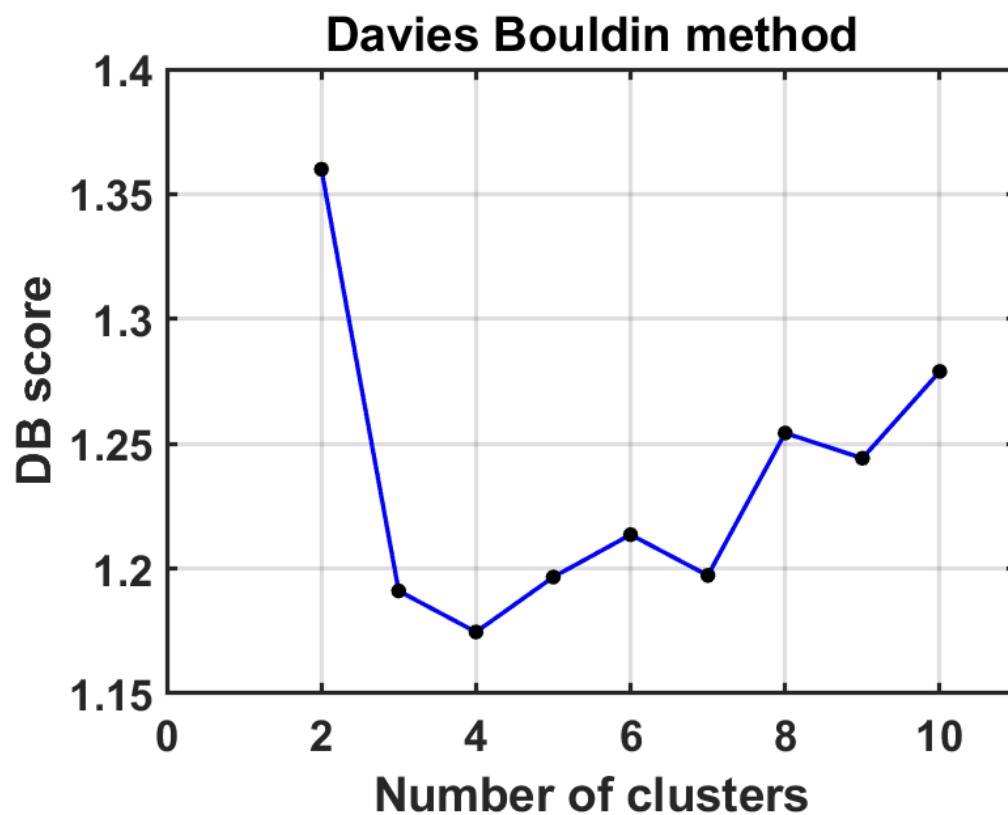
Figure S4. Spatial distribution of surface enhancement of HRRR rain liquid water content. Difference between mean rain liquid water content at (a) 1 km and 0.5 km; (b) 2 km and 0.5 km and (c) 3 km and 0.5 km AGL. High negative values indicate near-surface enhancement of precipitation tied to detection and estimation errors in GPM Ku-PR precipitation products.
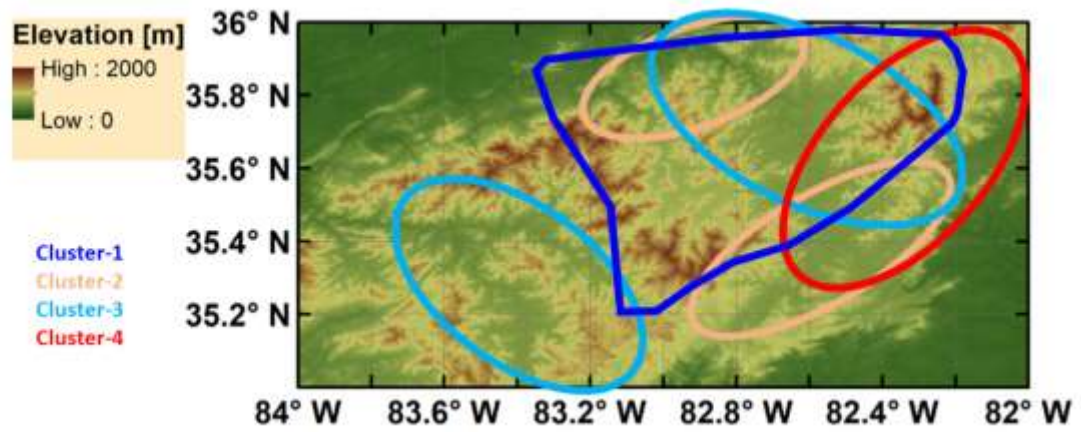
Figure S5. Example of GPM overpass on February 18, 2019 with large parallax errors in Ku-PR rainfall estimates compared to MRMS due to the large viewing angle.

Figure S6. Map showing the region of study at the Southern Appalachian Mountains (SAM) with locations of long-term rain-gauge network. The green, blue and red boxes denote western, inner and eastern region [from Arulraj and Barros, 2019].
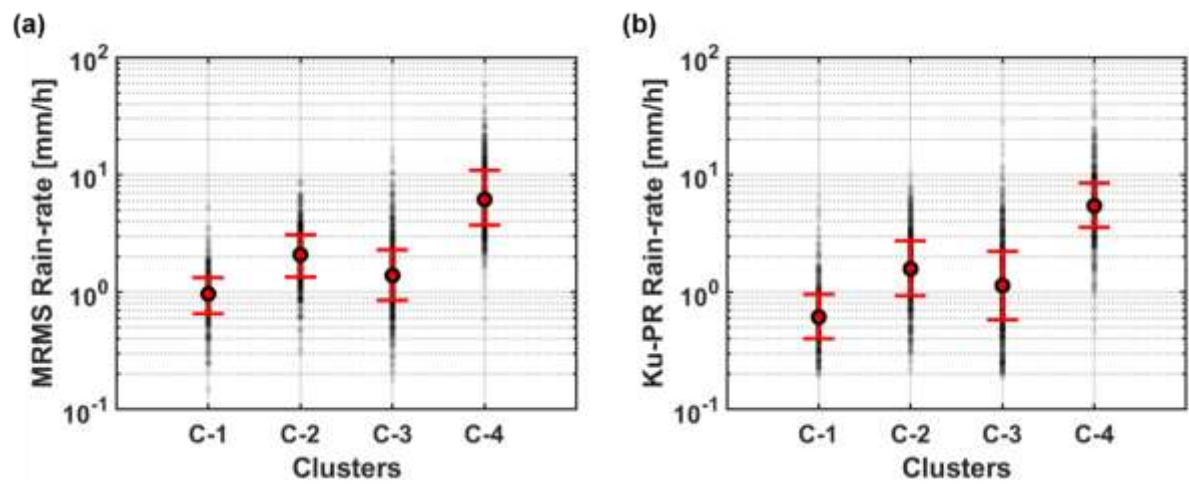
Figure S7. Davies-Bouldin (DB) index computed for different number of clusters of MRMS reflectivity features in the k-means algorithm.
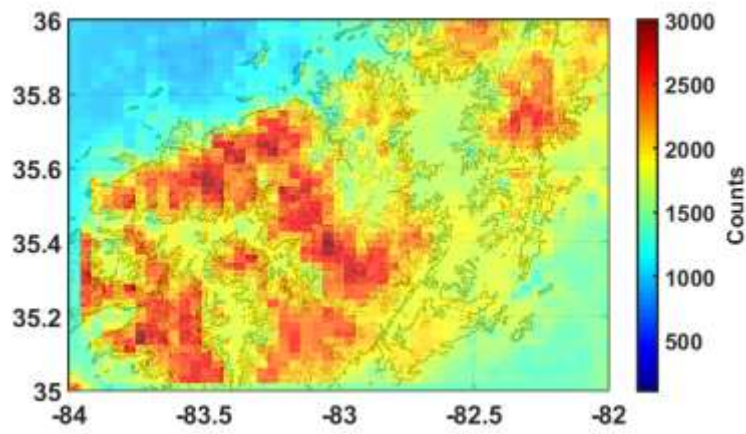
Figure S8. Synthesis of the spatial patterns of most frequent occurrences (hot-spots) of the four MRMS cluster classes.
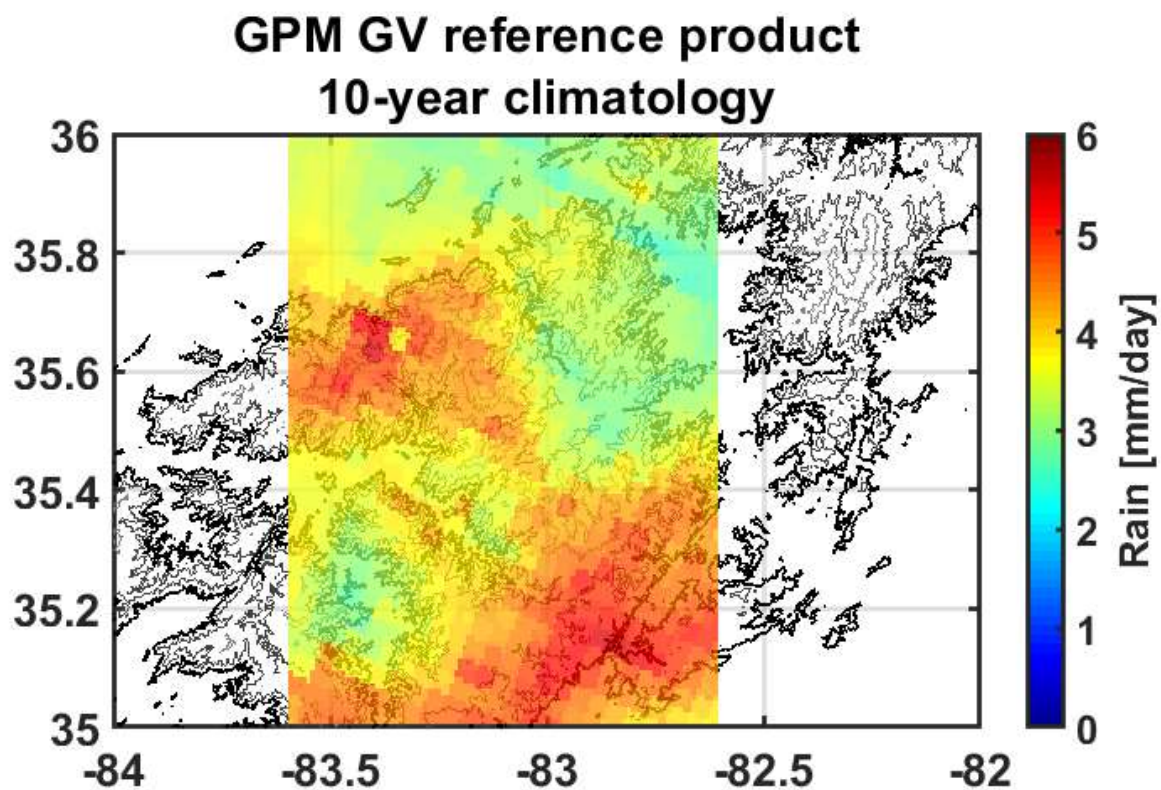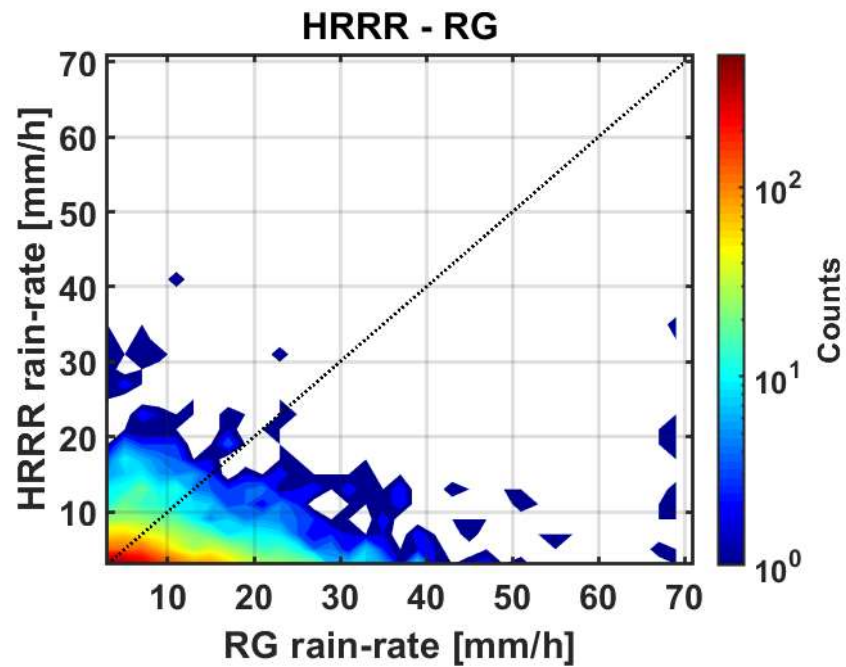
Figure S9. Concurrent mean precipitation rate (marker) with the standard deviation (error bars) for each of the MRMS clusters: (a) MRMS and (b) Ku-PR.

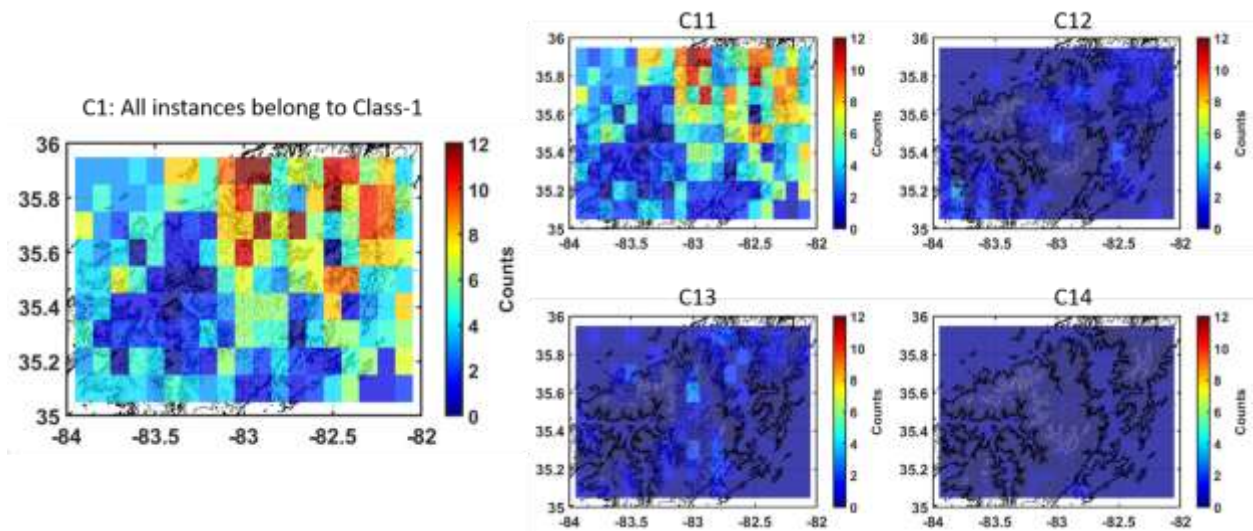**Figure S10**. Spatial distribution of HRRR precipitation frequency.

Figure S11. Spatial distribution of the 10-year average precipitation climatology from GPM GV reference precipitation product (Liao and Barros 2019).
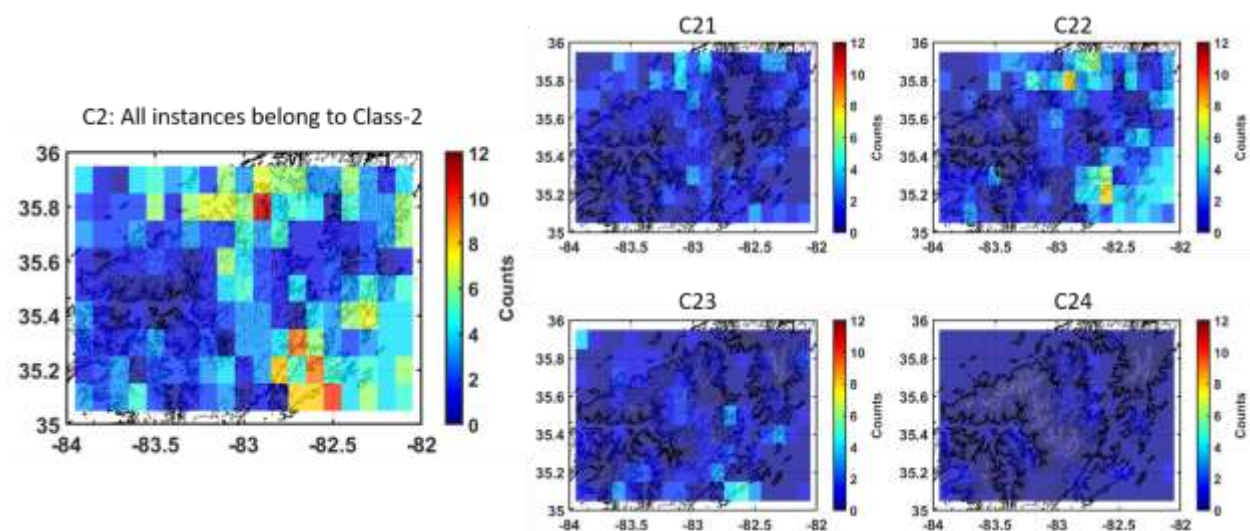
Figure S12. Density plot comparing the rain-rate derived from the rain-gauges with the HRRR simulated rain-rates at 500-m AGL.
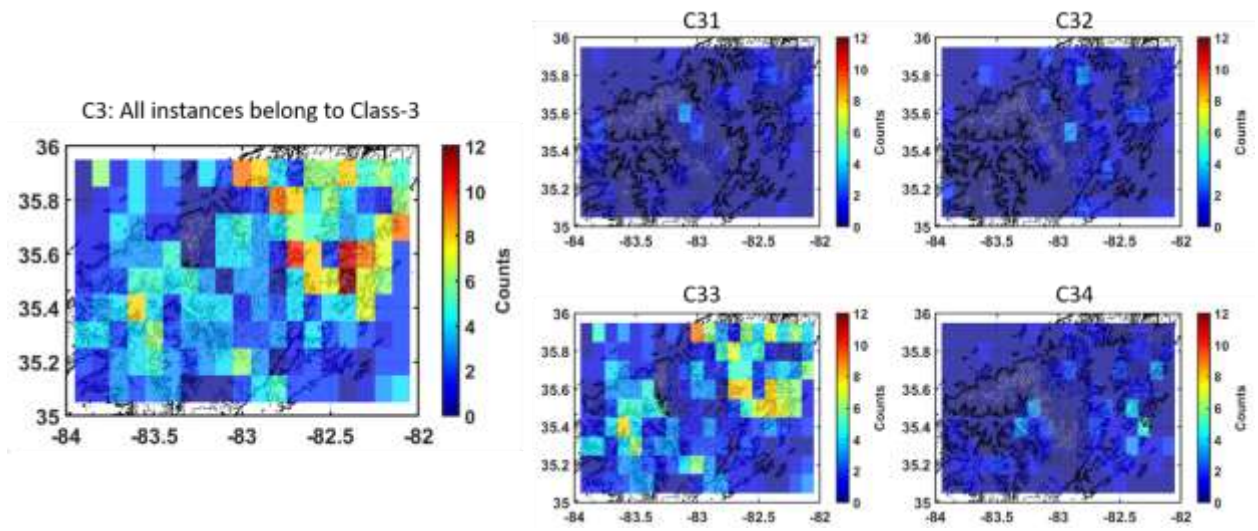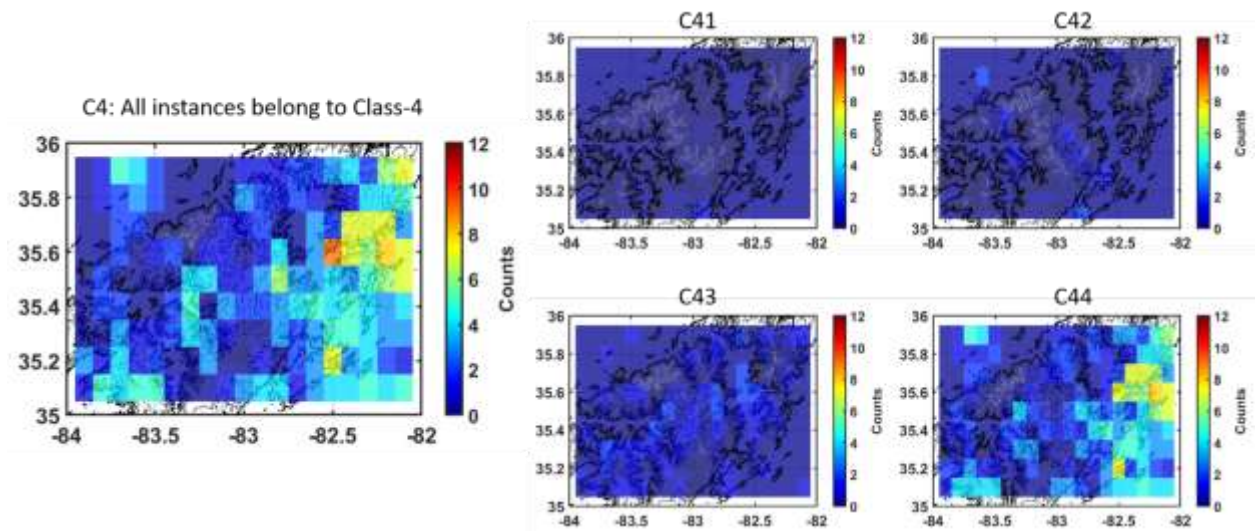
Figure S13. Left panel - Spatial distribution of MRMS Cluster-1 frequency of occurrence. Right panel – Spatial distribution of Cluster-1 GPM Ku-PR reflectivity profiles predicted by the precipitation classification algorithm. CXY denotes the output of the classification algorithm where X is the true class and Y is the model output.

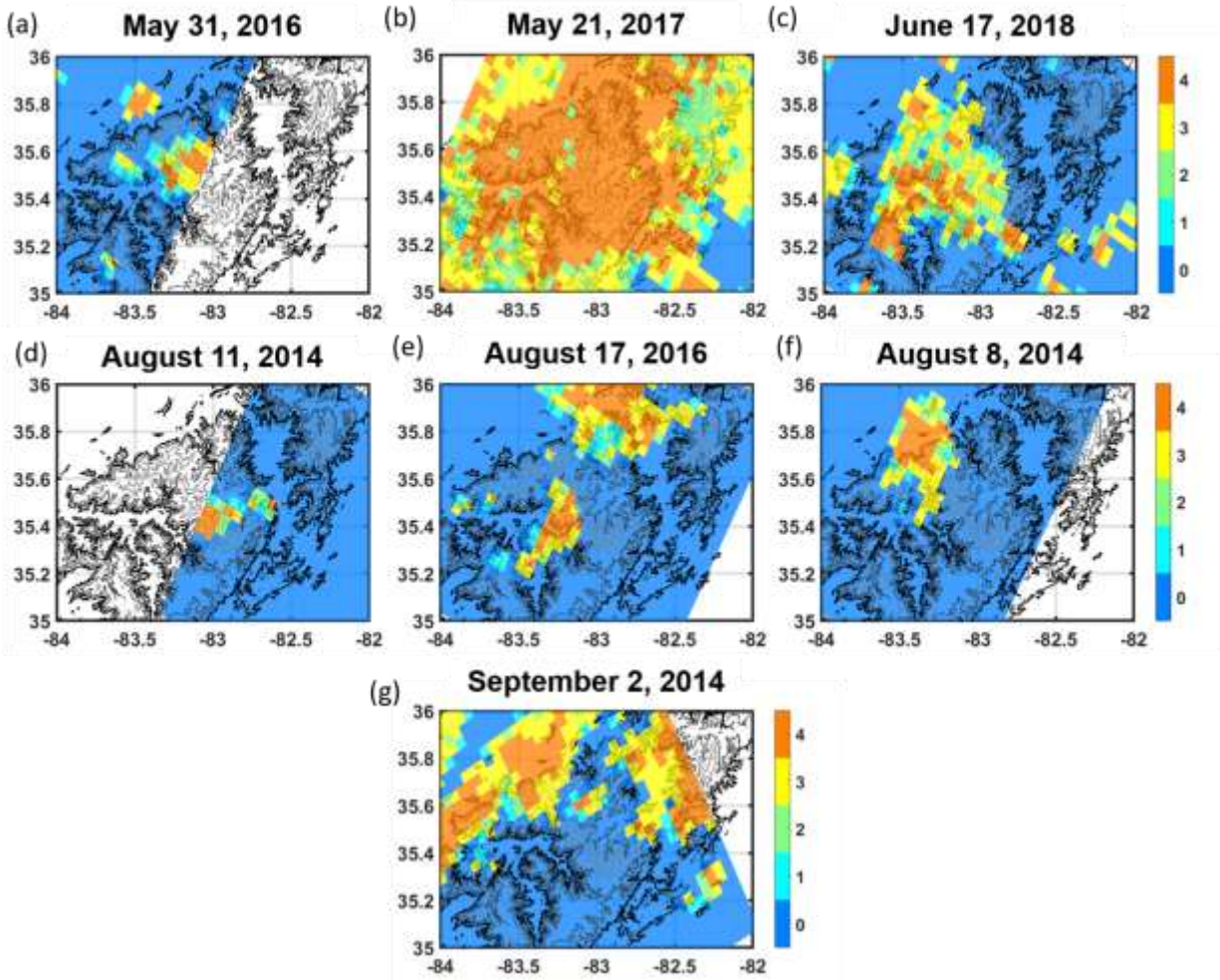**Figure S14.** Same as Fig. S13 but for Class-2.

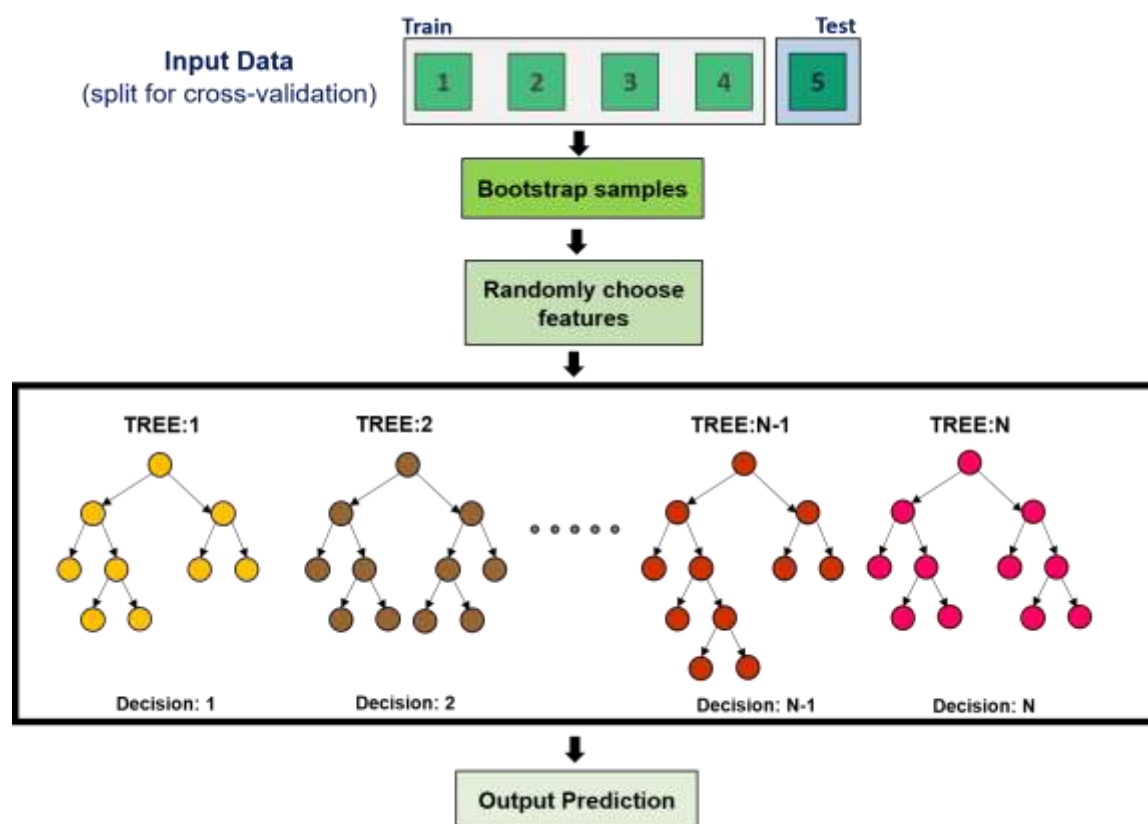**Figure S15.** Same as Fig. S13 but for Class-3.

Figure S16. Same as Fig. S13 but for Class-4.

Figure S17. Spatial distribution of predicted classification labels for GPM overpasses listed in Table 7. Legend: 0 - No rain ; X – Rain in Cluster-X, X=1,2,3,4.

Figure S18. Schematic representation of the Random Forest Classifier (RFC) used for precipitation detection.